Contrib Mineral Petrol (2001) 142: 147–162
DOI 10.1007/s004100100284

Roland Eichhorn · Georg Loth · Allen Kennedy

Unravelling the pre-Variscan evolution of the Habach terrane (Tauern Window, Austria) by U-Pb SHRIMP zircon data

Received: 18 April 2000 / Accepted: 15 May 2001 / Published online: 3 August 2001

Abstract The U-Pb SHRIMP age determinations of zircons from the Habach terrane (Tauern Window, Austria) reveal a complex evolution of this basement unit, which is exposed in the Penninic domain of the Alpine orogen. The oldest components are found in zircons of a metamorphosed granitoid clast, of a migmatitic leucosome, and of a meta-rhyolitic (Variscan) tuff which bear cores of Archean age. The U-Pb ages of discordant zircon cores of the same rocks range between 540 and 520 Ma. It is assumed that the latter zircons were originally also of Archean origin and suffered severe lead loss, whilst being incorporated into Early-Cambrian volcanic arc magmas. The provenance region of the Archean (2.64–2.06 Ga) zircons is assumed to be a terrane of Gondwana affinity: i.e., the West African craton (Hoggar Shield, Reguibat Shield). The Caledonian metamorphism left a pervasive structural imprint in amphibolite facies on rocks of the Habach terrane; it is postdated by discordant zircons of a migmatitic leucosome at < 440 Ma (presumably ca. 420 Ma). Alpine and Variscan upper greenschist- to amphibolite-facies conditions caused partial lead loss in zircons of a muscovite gneiss ('white schist') only, where extensive fluid flow and brittle deformation due to its position near a nappe-sole thrust enhanced the grains' susceptibility to isotopic disturbance. The Habach terrane – an active continental margin with ensialic back-arc development – showed subduction-induced magmatic activity approx. between 550 and 507 Ma. Back-arc diorites and arc basalts were intruded by ultramafic sills and subsequently by small patches of mantle-dominated unaltered and (in the vicinity of a major tungsten deposit) altered granitoids. Fore-arc (shales) and back-arc (greywackes, cherts) basin sediments as well as arc and back-arc magmatites were not only nappe-stacked by the Caledonian compressional regime closing the presumably narrow oceanic back-arc basin and squeezing mafic to ultramafic cumulates out of high-level magma chambers (496–482 Ma). It also induced uplift and erosion of deeply rooted crystalline complexes and triggered the development of a successor basin filled with predominantly clastic greywacke-arkosic sediments. The study demonstrates that the basement rocks exposed in the Habach terrane might be the 'missing link' between similar units of the more westerly positioned External domain (i.e., Aar, Aiguilles Rouges, Mont Blanc) and the Austroalpine domain to the east (Oetztal, Silvretta).

Dedicated to Prof. Dr. Rudolf Höll on the occasion of his 65th birthday.

R. Eichhorn (✉)
Bayerisches Geologisches Landesamt,
Heßstr. 128, 80797 Munich, Germany
E-mail: roland.eichhorn@stmlu.bayern.de

G. Loth
Institut für Allgemeine und Angewandte Geologie,
Luisenstr. 37, 80333 Munich, Germany

A. Kennedy
Curtin University of Technology,
GPO Box U 1987, Perth 6001, Australia

Editorial responsibility: J. Hoefs

Introduction

In recent years, Late-Precambrian to Ordovician relics of oceanic crust and subduction-related rocks were identified in basement areas of all four Alpine domains (i.e., the Southalpine, Austroalpine, Penninic and External domains). A tentative reconstruction of the palaeogeographic situation before the Variscan orogeny can even demonstrate that these relics follow a kind of linear distribution, which testifies subduction of oceanic domains along an active Gondwana margin (Raumer 1998). Moreover, Ordovician to Silurian arc-continent collision and crustal thickening is documented by granitoids and migmatites as well as acid volcanics, which record plate-tectonic evolution at higher crustal levels (Fig. 1).

In this paper we focus on a multiple-metamorphosed basement unit exposed in the Penninic Tauern Window – the 'Habach terrane' (Frisch and Neubauer 1989),

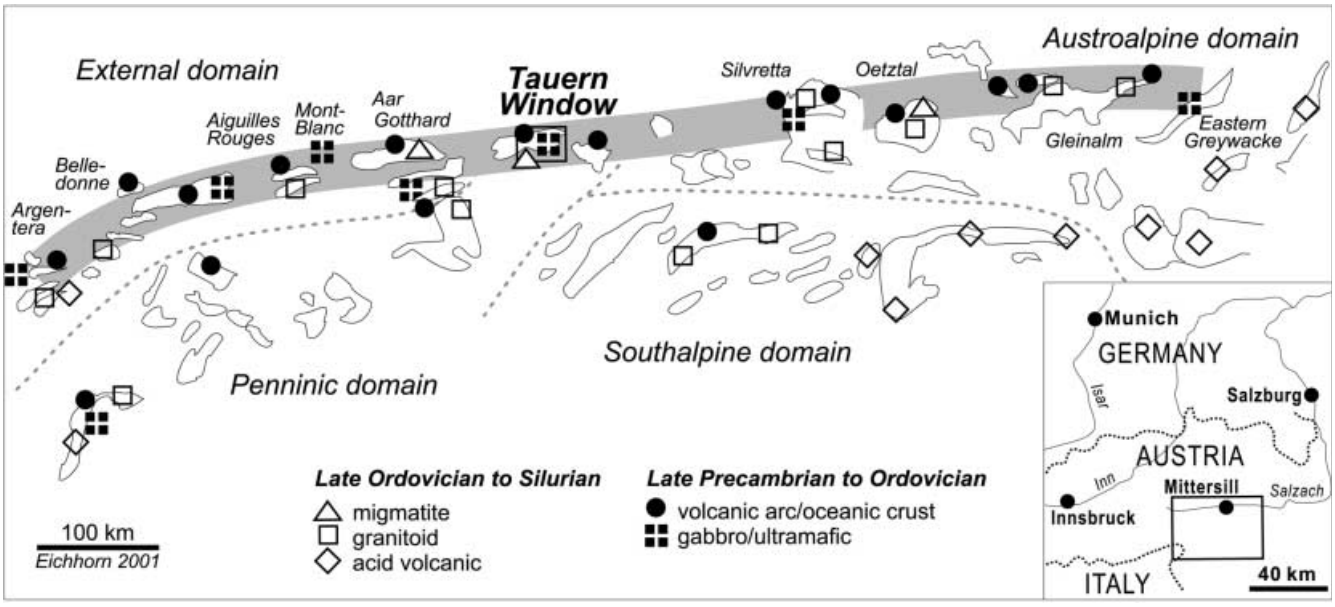

Fig. 1 According to palinspastic reconstruction (after Raumer 1998), the northern margin of the Intra-Alpine terrane comprises a longitudinal alignment (*shaded area*) of Precambrian to Ordovician subduction-related rocks, whereas Late-Ordovician to Silurian leucocratic rocks prevail more to the south. *Framed area* of the Tauern Window is enlarged in Fig. 2a

which serves as a junction between similar units of the External domain to the west and of the Austroalpine domain to the east, and which comprises the complete spectra of an active continental margin (accretionary wedge with slices of subducted fore-arc oceanic crust, main arc, ensialic back-arc oceanic basin with sedimentary cover; Eichhorn et al. 1999). Such a scenario, involving burial, exhumation, decompressional melting, in addition to the presence of inherited zircon cores and partial lead loss, demands age determinations which are both precise and of high spatial resolution. So far, our knowledge about the 'active life span' of this continental margin, from initial rifting towards accretion, is still rudimentary because age determinations which meet the above requirements are sparse. Therefore, cathodoluminescence images of zircons combined with SHRIMP analysis are used in order to gain geologically meaningful age information and, in consequence, to decipher the complex pre-Variscan history of the Habach terrane in greater detail.

Geology and sample selection

The Habach terrane is situated in the northeastern part of the Penninic domain of the Central Alps (Fig. 1). Early-Alpine compressional tectonics nappe-stacked its rocks and buried them further below nappes of the Austroalpine domain. Late- and post-Alpine uplift and exhumation created a tectonic window (Tauern Window) where the present outcrops are exposed. The terrane consists of Ordovician to Late-Precambrian basement rocks which were intruded by large volumes of Permo-Carboniferous granitoids (e.g., Granatspitz, Tux, and Venediger) and overlain by coeval volcanics and sediments (Eichhorn et al. 2000; Fig. 2).

The basement rocks can be divided into two units based on different lithological contents reflecting different geotectonic environments: (1) the Stubach Group as ensialic back-arc oceanic basin with sedimentary cover, and (2) the Habach Group comprising slices of subducted fore-arc oceanic crust accreted to the main volcanic arc (Eichhorn et al. 1999).

Stubach Group

The predominantly magmatic rocks of the ensialic back-arc basin are exposed in several large units (Sturmmannseck and Zwölferzug north of, Basisamphibolit around and Abretterkopffolge southwest of the Granatspitz massif) which have been referred to as 'magmatic formation' in Fig. 2. Its main rock types are (coarse-grained) amphibolites and hornblende-plagioclase gneisses, hornblendites, muscovite-plagioclase gneisses, muscovite gneisses, porphyroid gneisses and some ultramafic bodies as well as very rare occurrences of metasediments (paragneisses, micaschists and marbles; Loth and Höll 1994). Similar metasediments cover the magmatites and are exposed in several minor unnamed outcrops northwest of, in the Basisschieferfolge around, and in the Serie der Alten Gneise south, southwest and southeast of the Granatspitz massif (cf. 'sedimentary formation' in Fig. 2). The metasediments comprise a sequence of alternating and interfingering micaschists and paragneisses (meta-greywackes). Minor intercalations consist of amphibolites and leucocratic orthogneisses, rare quartzites, marbles, meta-conglomerates and meta-breccias.

The hornblende-plagioclase gneisses (sample SG-1) form intercalations within the amphibolites, varying from a few centimeters to more than one meter in thickness. They contain medium-grade Variscan metamorphic mineral relics (hornblende, garnet, plagioclase). Amphibolites and hornblende-plagioclase gneisses have usually not been separated but rather described as one lithological unit, called 'banded amphibolites', which has been

Fig. 2 **a** Geological map of the central Tauern Window, and **b** schematic cross section in down-plunge view projected to line A-A′. *Closed circles* with numbers and expression '1-6' indicate sample localities of Stubach Group and Habach Group rocks, respectively, as compiled in Table 2. Note that Early-Alpine (and presumably Variscan) compressional tectonics nappe-stacked its lithologies, so that the Granatspitz autochthon(?) has been overridden by the Tux and Venediger nappes. Pre-Cambrian to Cambrian microfossil finds are indicated by *stars*

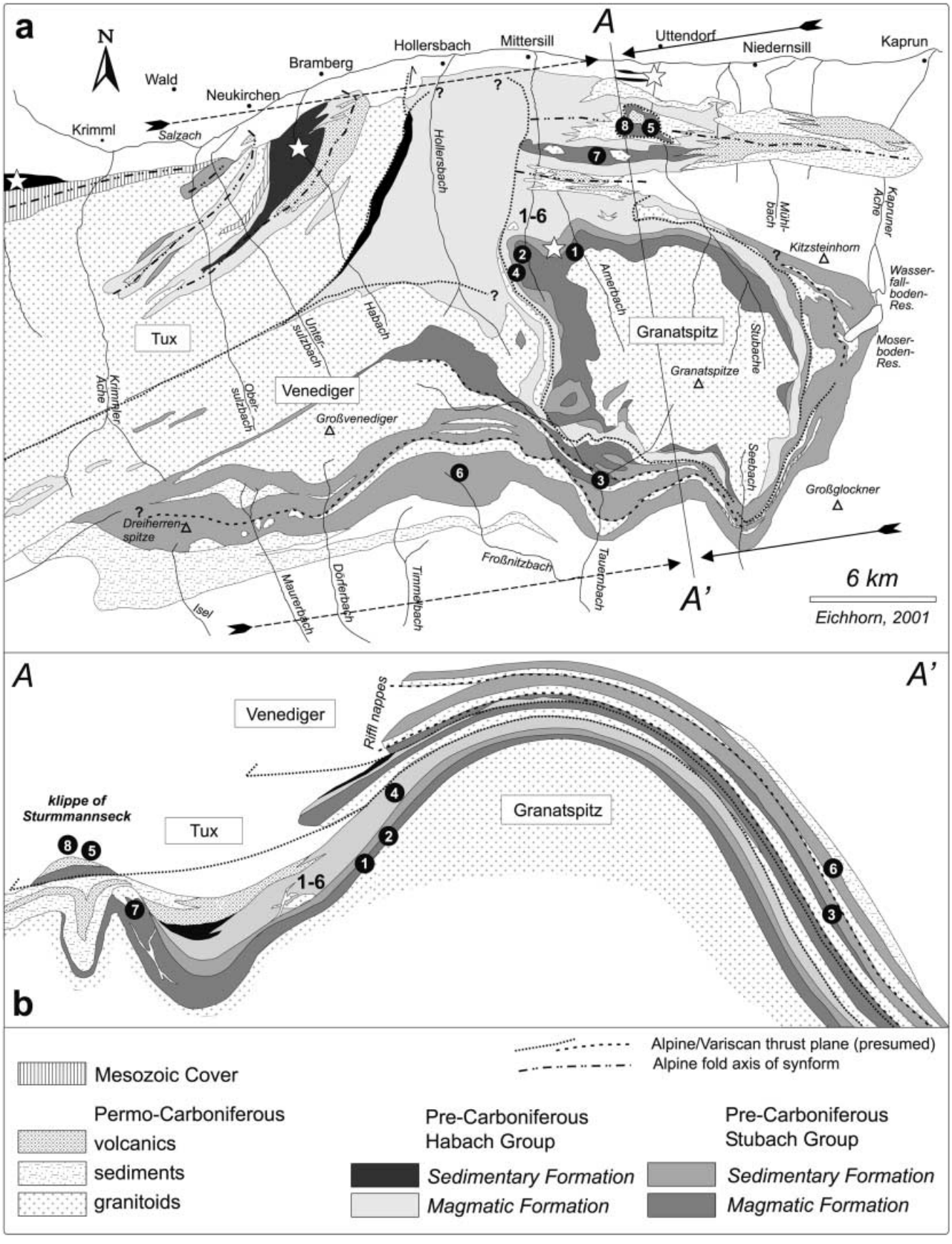
a
N
A
A'
Hollersbach
Mittersill
Uttendorf
Niedernsill
Kaprun
Bramberg
Wald
Neukirchen
Krimml
Salzach
Hollersbach
1-6
Mühl-bach
Kapruner Ache
Kitzsteinhorn
Wasser-fall-boden-Res.
Moser-boden-Res.
Ameibach
Granatspitz
Stubache
Granatspitze
Tux
Unter-sulzbach
Habach
Venediger
Ober-sulzbach
Krimmler Ache
Großvenediger
Seebach
Großglockner
Dreiherren-spitze
Frossnitzbach
Tauernbach
Dörferbach
Timmelbach
Maurerbach
Isel
6 km
Eichhorn, 2001
b
A
A'
Venediger
Riffl nappes
klippe of Sturmmannseck
Tux
Granatspitz
1-6
Alpine/Variscan thrust plane (presumed)
Alpine fold axis of synform
Mesozoic Cover
Permo-Carboniferous
volcanics
sediments
granitoids
Pre-Carboniferous
Habach Group
Sedimentary Formation
Magmatic Formation
Pre-Carboniferous
Stubach Group
Sedimentary Formation
Magmatic Formation

formed by Variscan anatexis and/or metamorphic segregation. On the contrary, Loth and Höll (1994) inferred two different magmatic rock types of pre-Variscan age and rejected the idea of Variscan anatexis based on petrographical and zircon morphological studies. Loth et al. (1997) further argued that the two rock types may have formed either coeval in a layered intrusion or ophiolite complex, or noncoeval where the crustal dioritic precursor of the hornblende-plagioclase gneiss has been intruded by gabbroic sills in the wake of initial (back-arc?) rifting. Sample SG-1 has been chosen to resolve this age problem by comparing our radiometric data with existing gabbro (now metamorphosed coarse-grained amphibolites and garnet amphibolites) formation ages.

The muscovite gneisses (sample SG-5) are characterized by a modal composition of about 70% quartz, 10% muscovite and 10% albite ('white schists'). The high content of quartz is interpreted as resulting from the breakdown of alkali feldspar during metamorphism and deformation. Muscovite gneisses have been found only near an occurrence of poophyroid gneisses (sample SG-8) in the Sturmmannseck, and have thus at first been interpreted as tectonized equivalents (Hammer 1937). Field geological, petrographical and zircon morphological studies subsequently revealed that the muscovite gneisses are alkaline granitoid intrusives of mainly mantle origin, whereas the porphyric texture of the latter with many rock fragments and magmatic mineral relics, its wealth of xenocrysts and inherited zircon cores, and its nondeformed appearance affirms its presumably Variscan volcanic origin (Loth and Höll 1994). The high deformational degree of the muscovite gneisses may be explained by the fact that they occur near the nappe sole thrust of a tectonic klippe of the Tux nappe (Fig. 2b). The two samples SG-5 and SG-8 were studied in order to get some information of the later evolution of the convergent plate margin and of the provenance age(s) of the source rocks, respectively.

Lensoid occurrences of meta-conglomerates within the 'sedimentary formation' reveal elongated, seldom well-rounded clasts embedded within fine-grained biotite-plagioclase gneisses or plagioclase-biotite schists. The clasts consist of amphibolites, various leucocratic schists and gneisses, marbles and quartzites. Sample SG-4 is a huge 40-cm leucocratic orthogneiss clast which derived from a 1.4-m thick, unsorted meta-breccia of gneisses and amphibolites. The deposition mechanism of the breccias and conglomerates is still a matter of debate. Gilg et al. (1989) considered a deposition by debris and mud flows triggered by local submarine earthquakes and/or a deposition by drifting icebergs. The former interpretation is corroborated by the broad variety of clasts, the latter by the finds of some exotic, large single clasts which were interpreted as dropstones from melting icebergs, embedded in fine-grained laminated sediments (now metamorphosed biotite-plagioclase gneisses). We dated the orthogneiss clast to gain some information about the age of the orthogneiss protolith and, in consequence, to get an upper estimate for the deposition time of the meta-breccia.

Additionally, we dated a migmatitic leucosome (SG-3) from the Serie der Alten Gneise to elucidate the time of migmatization. Variscan nappe-stacking (Riffl nappes; Fig. 2b) produced a heterogeneous association of pre-Variscan Stubach Group rocks in form of high-grade gneisses, migmatites and (eclogitic) amphibolites together with Variscan, 340-Ma-old 'in-situ' anatexites. Eichhorn et al. (1999) argued that the formation time of the anatexites may be identical to the time of migmatization of the Stubach Group rocks. This interpretation is further corroborated by the fact that the Variscan amphibolite-facies metamorphism is regarded as comparable to, or even more intense than Alpine lower amphibolite-facies conditions (Eichhorn et al. 1995), and that the thermal peak of the Variscan metamorphism occurred between 324 and 282 Ma (Höll and Eichhorn 2000). On the other hand, ages between 415 and 422 Ma from (eclogitic) amphibolites have been interpreted to indicate a high-pressure metamorphism which converted these gabbros into eclogites during a Silurian subduction (Quadt et al. 1997).

Habach Group

The volcanic arc rocks of the Habach Group, referred to as 'magmatic formation', consist mainly of fine-grained amphibolites, minor hornblendites and coarse-grained amphibolites as well as various leucocratic gneisses. The basaltic protoliths of the fine-grained amphibolites were intruded by pyroxenitic and gabbroic melts as well as small patches of normal 'I-type' granitoids and later by altered, differentiated granitic melts (Eichhorn et al. 1999; Höll and Eichhorn 2000). Slices of subducted fore-arc oceanic crust, which have been accreted to the main volcanic arc ('sedimentary formation'), comprise an up to 700-m-thick sequence of dark phyllites as well as minor micaschists and quartzites, locally intercalated with metavolcanics and ultramafics. The ultramafics represent remnants of oceanic crust which differ geochemically from Stubach Group equivalents (Puhl et al. 1998). The finds of various well-preserved microfossils in the dark phyllites describe a sedimentation period of Late Riphean to Early Vendian (i.e., 1.0–0.6 Ga; Reitz and Höll 1988; Reitz et al. 1989; Gilg et al. 1989).

Hornblendites and coarse-grained amphibolites (HG-6) form numerous, parallel to subparallel lenses, up to some meters thick. Gradual transitions as well as distinct contacts between the two cogenetic rock types have been described by Höll (1975). The amphiboles comprising 75–98 vol% of these dark-green hornblendites are mainly composed of brownish cores of Ti-rich tschermakitic to Mg-hornblende within actinolitic hornblende. Accessory minerals are scheelite, biotite, plagioclase, carbonate, epidote-group minerals, magnetite, hematite, ilmenite, Cr spinel, and some sulfides (Höll and Eichhorn 2000). The coarse-grained amphibolites contain less amphibole but up to 50 vol% plagioclase, together with the same minor to trace minerals. We dated a scheelite-poor coarse-grained amphibolite to serve as a crosscheck for the 'banded amphibolite' data of the Stubach Group rocks and as a reference for published ages of the hornblendites.

Methods

The samples comprised 5–30 kg of fresh material. Mineral fractions for isotopic analyses were processed through conventional mineral separation techniques, including a Wilfley table, heavy liquids and the Frantz isodynamic separator. Final mineral separates consisted of handpicked, top-quality zircon grains, homogeneous in terms of transparency, color and fluorescence.

Zircon grains from the sample and a zircon standard are mounted and polished in a 24-mm diameter epoxy disc and gold coated. The zircons are then photographed, examined by cathodoluminescence (CL) imaging and analyzed using the SHRIMP II ion microprobe. During data reduction, correction for common Pb in the zircon uses the methods of Compston et al. (1984). The calculation of $^{206}Pb/^{238}U$ ages is based upon the assumption that the bias of the measured $^{206}Pb^{+}/^{238}U^{+}$ ratio relative to the true ratio can be described by the same power law relationship (Claoue-Long et al. 1995) between $^{206}Pb^{+}/^{238}U^{+}$ and UO^{+}/U^{+} for both the CZ3 standard zircon (Pidgeon 1997) and the unknown zircon analysis. The uncertainty of the $^{206}Pb/^{238}U$ age of the unknown zircon includes the uncertainty of the $^{206}Pb^{+}/^{238}U^{+}$ ratio of the standard. For this reason, approximately twice the number of 'standard' analyses are interspersed between 'unknowns' analyses in any analytical session. Reproducibility for the 'standard' Pb/U ratio ranged between ± 1.05 and $\pm 2.22\%$ for the five SHRIMP sessions required to analyze the samples. The concentrations of U, Th and Pb are calculated using a similar approach to that used for the calculation of U/Pb ratios, with the unknown referenced to the standard with known U, Th and Pb abundances (Compston et al. 1984; Claoue-Long et al. 1995; Williams et al. 1996).

The zircons were examined with a Zeiss DSM 960A scanning electron microscope (SEM) at the Institut für Allgemeine und Angewandte Geologie, University of Munich, and with a JEOL 6400 at the Electron Microscopy Centre, University of Western Australia, Perth, in cathodoluminescence (CL) mode on polished and gold- or carbon-coated grain mounts for internal structures. The CL information was obtained prior to the SHRIMP analyses, in order to select appropriate zircons for analysis, to place the ion beam without straddling different zones within the same grain, and

to avoid 'bleached' zones of enhanced CL emission which are typical for areas with a disturbed U-Pb system (Pb loss).

Errors cited for individual analyses include errors from counting statistics, common ^{208}Pb or ^{204}Pb correction, and U-Pb calibration error based on reproducibility of U-Pb measurements of the standard. They are at the 1S level. Mean concordia ages given on grouped analyses and concordia-intercept ages are at the 95% confidence level. Intercept ages have been calculated with Isoplot/Ex Version 2.2 (Ludwig 2000). If not otherwise indicated, individual ages are always quoted as $^{206}Pb/^{238}U$ ages, bearing in mind that the $^{206}Pb/^{238}U$ error is generally the smallest error, because $^{206}Pb/^{238}U$ dates for SHRIMP analyses of Proterozoic to Paleozoic zircons are more precise than $^{207}Pb/^{235}U$ and $^{207}Pb/^{206}Pb$ dates, due to the lower abundance of ^{207}Pb as compared with ^{206}Pb in such zircons. Decay constants used are those recommended by IUGS (Steiger and Jäger 1977). The terminology of periods and epochs quoted herein follows the chronostratigraphic time scale of Gradstein and Ogg (1996).

Results

The zircon population of the hornblende-plagioclase gneiss (SG-1) displays CL structures which are characteristic for post-crystallization disturbance: the subhedral zircons in Fig. 3a reveal a dark, rounded internal domain with oscillatory to parallel zoning, rimmed by a broadly zoned domain. These broad zones show enhanced CL intensity ('bleaching') gradually fading out the primary structure. Progressive fading of zones correlates with reduction in Th and U and lowering of the Th/U ratio, which requires a lattice reorganization process enabling trace-element mobility. Many of the zone boundaries are nonplanar and convex, suggesting the migration of a replacement front from the margin towards the center of the grain. The SHRIMP data points of the primary and bleached growth zones yielded a single group with a concordant mean $^{206}Pb/^{238}U$ age of 551 ± 9 Ma. This mean age, interpreted to represent primary magmatic growth, might still be slightly biased by lead loss. Two spot analyses (1.2, 5.1) with lower ages were discarded from mean age calculation, because the CL investigation indicated enhancement of CL emission and recrystallization. The sector-zoned spot 5.1 has the lowest U and Th values and Th/U ratio (i.e., a 'metamorphic' ratio < 0.1 according to Heaman et al. 1990; Schaltegger et al. 1999).

Generally, the muscovite gneiss (SG-5) yields small zircons (80–120 μm) which are colorless, euhedral and often broken. Profound recrystallization ('cauliflower structures') of originally oscillatory zones is prominent under CL (Fig. 3b). In fact, it was almost impossible to place the SHRIMP beam on undisturbed growth zones. However, bleached and curved growth zones, which have been considered typical for the hornblende-plagioclase gneiss, are missing. Completely recrystallized grains (1 to 4) yield low Th and U values, with 21–146 ppm Th and 659–1,568 ppm U relative to analyses 5 to 11, and lower Th/U ratios of 0.22–0.01. Uranium and thorium contents of the analyzed non-recrystallized zircons are very high, varying in the range 460–1,327 ppm Th and 1,580–3,127 ppm U. As commonly observed in strictly magmatic zircons, grains with the lowest U content display the oldest ages due to smaller degrees of Pb loss in less metamict grains (radiation damage). Obviously, the recrystallization phenomena induced severe lattice destruction and enhanced leaching processes, thus triggering Th and U depletion. After rejection of these spots, a reference line passing through 8-10-5-6-11 gives an upper intercept age of 507 ± 39 Ma (Fig. 4b). Some of the recrystallized grains align on the reference line, others are concordant at 378 Ma (spot 2) and 359 Ma (spot 4) or reverse-discordant (spot 1.1).

Zircons from the porphyroid gneiss (SG-8) are very variable, from short to long prismatic, subhedral and clear. Strong oscillatory zoning, often around an inherited core, is the prominent growth type and probably represents growth in a melt phase (Fig. 3c). All analyses from strongly zoned areas plot analytically concordant with 279 ± 4 Ma. The inherited cores mainly reflect Proterozoic to Archean inheritance with $^{207}Pb/^{206}Pb$ ages of 0.5–0.6, 0.8, 1.6–1.7 and 2.4–2.5 Ga, whereas xenocrysts plot analytically concordant at ca. 330, 410 and 470 Ma.

The zircons from the gneiss clast (SG-4) are subhedral and 60–210 μm long. Surface corrosion interpreted as metamorphic dissolution phenomena is frequent. Enhancement of CL emission ('bleaching') and concurrent fading of pre-existing structures in some zircons clearly indicate a disturbance of the U-Pb system (Fig. 3d), although Th/U ratios well above 0.4 indicate magmatic values. Twelve analyses plot analytically concordant in a single group, displaying a mean $^{206}Pb/^{238}U$ age of 500 ± 6 Ma (Fig. 4c). The date may be slightly rejuvenated due to some spot positions in 'bleached' or faded growth zones, which is characteristic for loss of U, commonly coupled with a partial resetting of the U-Pb system (Vavra et al. 1996; Schaltegger et al. 1999). Two spot analyses (9.2, 5.2), derived from an unmixed zone quenching the CL emission (2,474 ppm U) and a completely recrystallized sector zone, respectively, result in $^{206}Pb/^{238}U$ ages as young as 456 ± 6 Ma. In Fig. 3d, even some of the magmatic inherited cores (3.1, 5.1) are almost completely reset, although the magmatic Th/U ratio was (partially?) preserved in grain 5. The other inherited cores yield Proterozoic to Archean $^{207}Pb/^{206}Pb$ ages of 0.6–0.7 and 1.8–2.1 Ga.

The migmatitic leucosome (SG-3) data display a large spread of points (Fig. 4d). The zircon population contains mostly subhedral equant grains, but perfectly euhedral grains of bipyramidal and prismatic shape can be found, too. CL images reveal oscillatory zoning and prominent relic cores (Fig. 3e). The uranium

Fig. 3a–f Cathodoluminescence images of zircons analyzed by ion microprobe (spot locations and numbering as well as SHRIMP ages are indicated). **a** Hornblende-plagioclase gneiss (SG-1). **b** Muscovite gneiss (SG-5). **c** Porphyroid gneiss (SG-8). **d** Gneiss clast of meta-breccia (SG-4). **e** Migmatitic leucosome (SG-3). **f** Coarse-grained amphibolite (HG-6). The ion-microprobe data are given in Table 1. *Length bar* = 50 μm

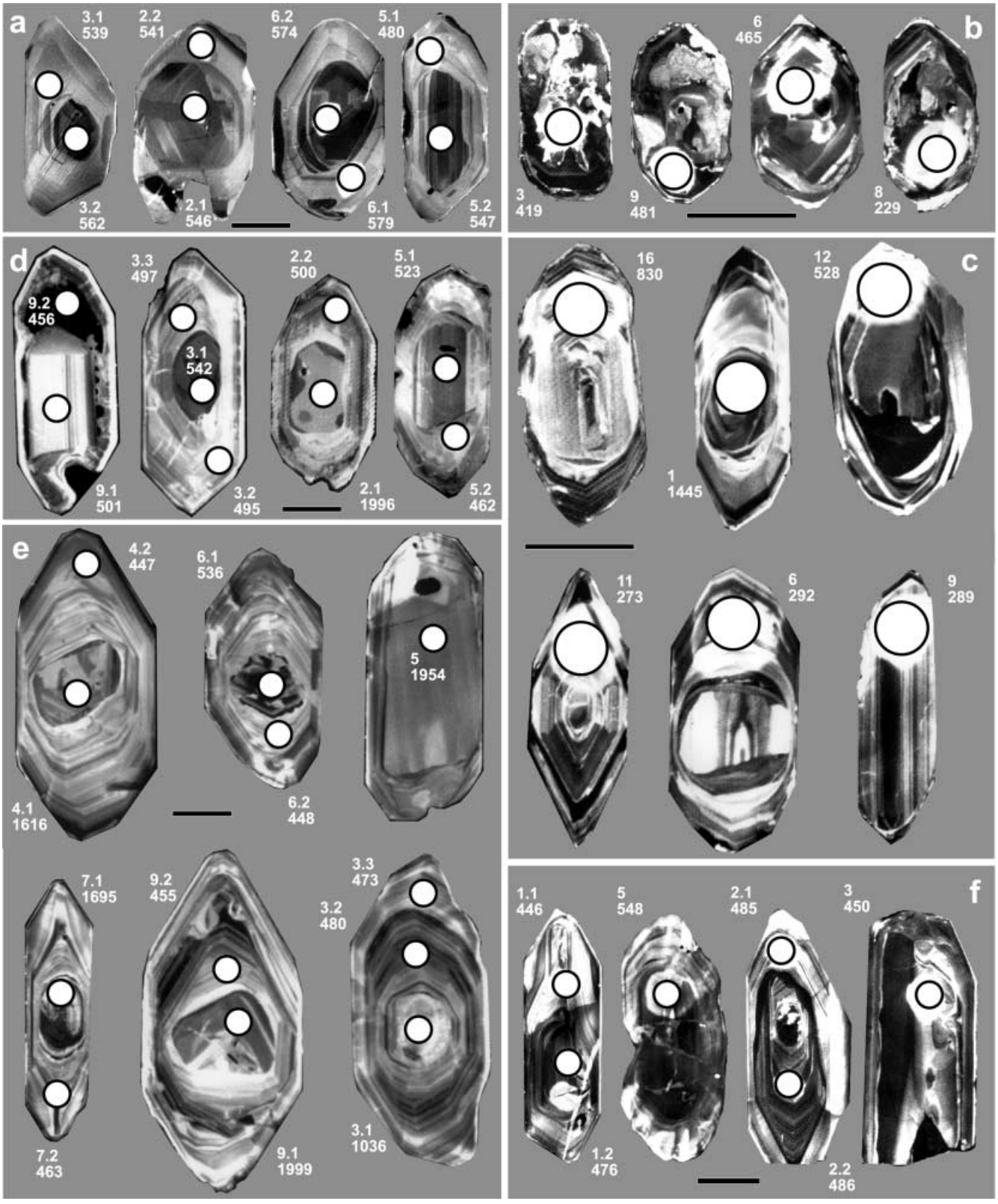

concentrations for the oscillatory zones scatter between 329 and 1,461 ppm, and Th/U ratios are mostly below 0.1, typical for metamorphic zircons (Schaltegger et al. 1999). They are thought to have crystallized or overgrown in the anatectic liquid. Grouping the five lowest SHRIMP data points (4.2, 6.2, 8.2, 1, 9.2) placed in oscillatory zones would result in a slightly discordant mean age of 449 ± 7 Ma (94% concordance). Four fur-

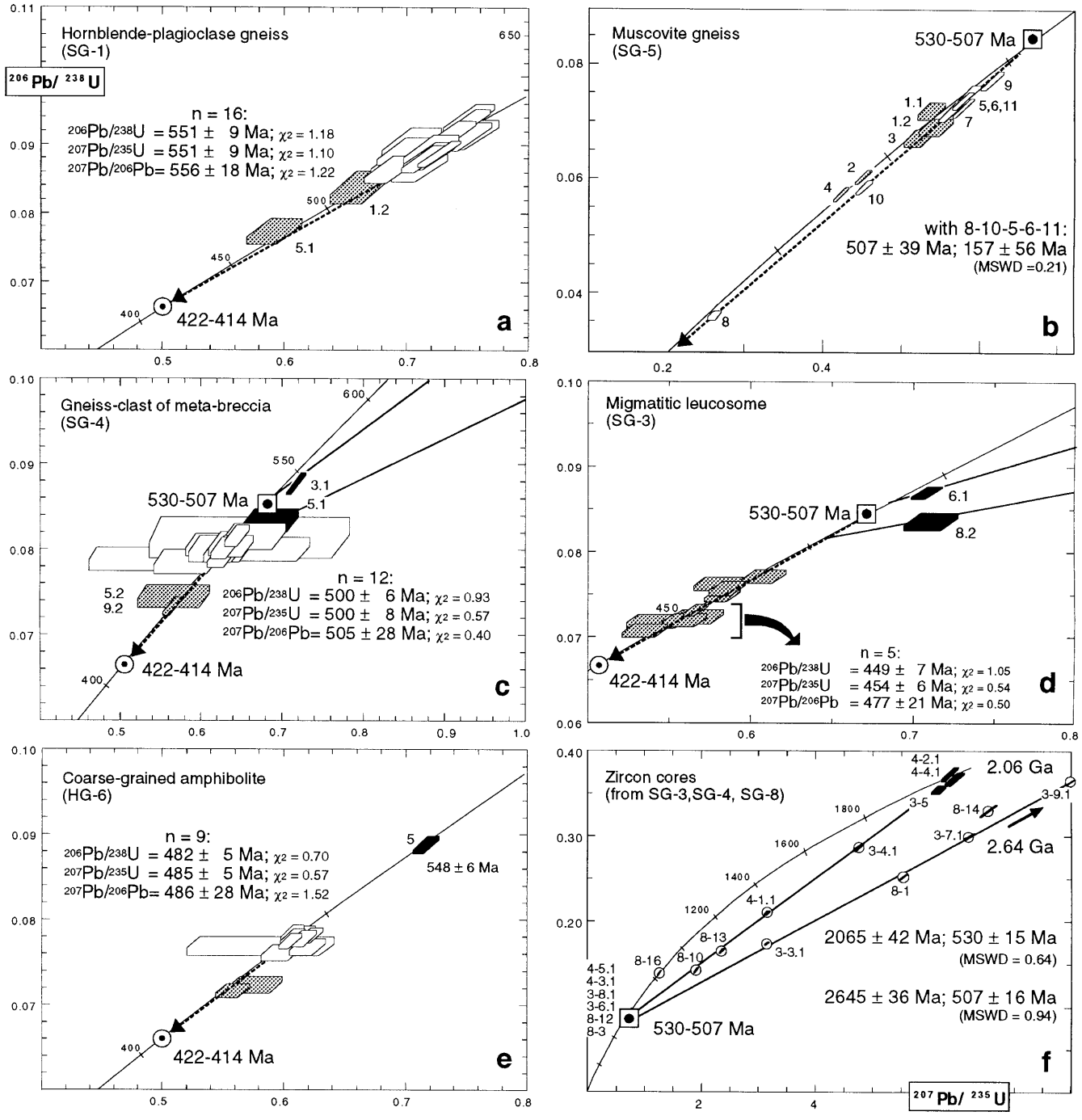

Fig. 4a–f Concordia diagrams displaying ion-microprobe data corrected for common Pb contribution. *Closed areas* Analyses of inherited cores or xenocrysts. *Shaded areas* Analyses which were discarded from the calculation on the basis of CL structures or – if *bracketed* – which produce lead-loss biased, slightly discordant data cluster. Error polygons are at the 1S level; all mean ages are at the 95% confidence level. *Dashed line with arrow* Hypothetical Pb-loss line towards thermal event

ther analyses (2, 3.2, 3.3 and 7.2) from oscillatory zones are analytically concordant to slightly (inverse-) discordant, but would also fit on a hypothetical lead-loss line. The inherited cores are of magmatic origin and mainly reflect Proterozoic to Archean inheritance with $^{207}Pb/^{206}Pb$ ages of 0.6–0.7, 2.0–2.1 and 2.5–2.6 Ga.

Zircons of the coarse-grained amphibolite (HG-6) reveal reddish oxidation overgrowths, although the internal color is whitish-clear. They are euhedral and long prismatic. CL structures are comparable to the ones of the hornblende-plagioclase gneiss (sample SG-1): A (partly) rounded, dark internal domain with oscillatory zones is overgrown by a thin rim with planar (oscillatory) growth zoning (Fig. 3f). These planar zones show enhanced CL intensity ('bleaching') combined with reduced Th and U contents and lowered Th/U ratios (cf.

grain 2). Nine pooled analyses from oscillatory zones give a slightly discordant mean age of 482 ± 5 Ma. Two further discordant spot analyses with ages as young as 446 ± 5 Ma may fit on a hypothetical lead-loss line (Fig. 4e).

Discussion

Silurian metamorphism

CL images of zircons of the hornblende-plagioclase gneiss (SG-1), the gneiss clast of the meta-breccia (SG-4), the migmatitic leucosome (SG-3) and the coarse-grained amphibolite (HG-6) reveal plenty of evidence for intense recrystallization (e.g., 'bleached' areas, curved growth zones, sector zoning, resorption fronts, 'black' zones quenching CL emissions). This suggests that such zircons were partially or completely reset by an important thermal event which occurred after their primary magmatic crystallization. Although many of these obviously rejuvenated zircons plot analytically concordant, they would also fit on a discordia line due to the flat curvature of the concordia which connects magmatic age and secondary thermal event (hypothetical lead-loss lines in Fig. 4a, c, d, e). Such a thermal event postdates the slightly discordant mean age of 449 ± 7 Ma from the migmatitic leucosome and might have taken place between 422 and 414 Ma according to recent works of Quadt et al. (1997; Sm-Nd garnet-whole rock: 422 ± 16 Ma; U-Pb zircon: 418 ± 18, 415 ± 18 Ma) and Raith et al. (2001; Re-Os molybdenite: 414.3 ± 1.6, 418.4 ± 1.6 Ma). Their samples as well as our aforementioned samples stem from an area which underwent the highest thermal overprint during the Alpine and Variscan metamorphisms, with temperatures reaching 590–600 °C (Hoernes and Friedrichsen 1974) and pressures of 10–12 kbar (Kupferschmied 1994). Yet, these amphibolite-facies p-T conditions could obviously not disturb the U-Pb systems of these zircons. This might be explained by the fact that these zircons had already recrystallized during an approx. 420-Ma-old 'Caledonian' thermal event, rendering them less sensitive to subsequent Pb losses in Variscan and Alpine times. This resistance was possibly supported by much lower U contents of samples SG-1, SG-4, SG-3 and HG-6 compared to the muscovite gneiss sample SG-5 (Table 1). A Caledonian metamorphism left a pervasive structural imprint in amphibolite facies on the rocks of the Aar massif west of the Tauern Window as well. It is dated at 456 ± 2 and ca. 445 Ma by zircons of a layered migmatitic gneiss and a migmatitic leucosome, respectively (Schaltegger 1993). Further high-pressure events are reported from eclogites of the Argentera and Belledonne massifs at 424 ± 4 and 395 ± 2 Ma, respectively (Paquette et al. 1989).

Sample SG-5 stems from the northern margin of the Tauern Window (klippe of Sturmmannseck) with lower Alpine temperatures not exceeding 500 °C (Hoernes and Friedrichsen 1974) and, thus, preserving Variscan amphibolite-facies mineral relics (Loth and Höll 1994). High degrees of discordancy in some grains (analyses 10 and 8 in Table 1) are due to exceptionally high U contents (2,969–3,127 ppm) which caused radiation damage. The good fit of the zircon analyses on a straight line towards a Variscan/Alpine thermal overprint does not necessarily indicate that the U-Pb system in these zircons was not disturbed during Caledonian metamorphism as well. The zircons have rather been more susceptible to the subsequent Variscan and Alpine recrystallization processes than all the other investigated samples due to their high U contents together with their position near the nappe sole thrust of the Sturmmannseck klippe, where extensive fluid flow and brittle deformation enhanced a complete resetting of their U-Pb isotopic systems.

Late-Precambrian to Cambrian magmatism

A major question for the interpretation of the U/Pb age results of the hornblende-plagioclase gneiss (SG-1), the gneiss clast of the meta-breccia (SG-4) and the coarse-grained amphibolite (HG-6) is whether the Caledonian thermal overprint rejuvenated not only the apparently recrystallized grains but also the population as a whole. Progressive recrystallization of oscillatory zoned zircons is accompanied by loss of U, Th and Pb and the removal of the oscillatory zones. Such recrystallized zircons are extremely stable with respect to later Pb loss and tend to retain concordant or slightly discordant U-Pb ages. The U-Pb age then dates the recrystallization event, which may be close to the age of primary crystallization or reflect a later metamorphism (Pidgeon 1992).

The hornblende-plagioclase gneiss (SG-1) yields a concordant mean age of 551 ± 9 Ma. On the one hand, this age can be regarded as minimum magmatic crystallization age of the dioritic precursor. Prominent recrystallization processes ('bleached zones') might have biased the analyses towards somewhat lower values, rendering the true magmatic age at approx. 580 Ma (spots 6.1 and 6.2). On the other hand, the grouped analyses without excess scatter and the identical spot ages within error limits between bright CL rims and dark oscillatory zoned centers favor an interpretation of the mean age as geological significant. Moreover, the age is coeval to the earliest basaltic volcanism reported from the main volcanic arc with 547 ± 27 Ma, rendering the subduction-induced arc and back-arc activities coeval. We tend to accept the latter interpretation, because arc and back-arc usually coexist in space and do not follow each other in time.

The gneiss clast of the meta-breccia (SG-4) defines a single zircon population without excess scatter, yielding a concordant mean age of 500 ± 6 Ma. The date is supposed to be rejuvenated due to some spot positions in 'bleached' or faded growth zones. However, the rejuvenation is presumably not very significant, because slightly discordant Cambrian zircon cores, which align

on two reference lines with lower intercepts at 530 and 507 Ma, give an upper estimate for their incorporation into the magma from which the gneiss clast derived. In addition, its volcanic-arc signature renders the source rock an integral constituent of the subduction-related rock suite. Granitoid source rocks intruded the metamorphic basement of the western Penninic domain as well, at 507 ± 9 Ma (granophyres) and at 500 ± 4 Ma (alkaline granites; Raumer 1998).

The mean age of the coarse-grained amphibolite (HG-6) is slightly discordant at 482 ± 5 Ma, but it nevertheless indicates an age range similar to magmatic ages reported from eclogitic and garnet amphibolites (488 ± 12 and 486 ± 5 Ma, respectively; Table 2). An interpretation problem arises from the concordant 'spot 5' age of 548 ± 6 Ma. Spot 5 derives from the recrystallized, dark and slightly rounded center area of a grain which is not interpreted as a xenocryst. Although the existence of inherited cores in gabbros and/or ultramafics is, to our knowledge, not reported so far, we tentatively interpret this feature as an inherited zircon core. This assumption is corroborated by field geological and radiometric evidence, because the precursors of the coarse-grained amphibolites intruded into a rock pile where approx. 540–550 Ma old zircons were common and could have been assimilated into the gabbroic melt (Table 2).

The nature of the Late-Archean and Cambrian detrital zircons

Most of the investigated, optically visible zircon cores from SG-3, SG-4 and SG-8 are mechanically rounded and/or chemically resorbed (Fig. 3c, d, e). They consist of discordant, originally Archean zircons (group I), and slightly discordant zircons around 530 Ma (group II; Fig. 4f). Two reference lines were calculated for the group-I zircons. The two lines bracket a provenance age of 2.06–2.64 Ga and an age of 507 to 530 Ma for a later disturbance of the U-Pb system of the zircons. Only one inherited core (8-16) with a concordant age of 830 ± 17 Ma shows an inheritance which is intermediate between 2.06 and 0.5 Ga. The scattering of the data points in Fig. 4f is presumably caused by lead loss during the subsequent multiple metamorphic overprints. Six group-II zircons have U-Pb ages ranging from ca. 540 to 520 Ma. Regressed together with the Archean group-I zircons, the six analyses are bracketed within error limits by the two reference lines with lower intercepts at 530 and 507 Ma. It is therefore assumed that the 530-Ma-old group-II zircons were originally also of Archean origin and suffered later severe lead loss whilst being incorporated into Early-Cambrian volcanic arc magmas.

Possible source rocks for these inherited Archean (and Meso-Proterozoic) zircons are located at the northern Gondwana margin. Igneous rocks which could have yielded 2.64, 2.06 and 0.8-Ga-old zircons are well documented in the Trans-Saharan mobile belt of the Hoggar Shield (Algeria) and in the Reguibat Shield (Morocco). The existing data suggest that 2.34 to 2.84-Ga metamorphosed rocks of the Reguibat Shield are intruded by 2.10–1.85 Ga old granites whereas the Hoggar Shield exposes 2.10–1.96 Ga and 870–840 Ma old granitoids (data compilation in Söllner et al. 1997).

The Habach terrane – from back-arc extension to arc-continent collision

The earliest ascertained magmatic activity in the Habach terrane started at about 550 Ma with the intrusion of diorites in the back-arc and the extrusion of basalts in the arc environment. These rocks were later intruded by gabbros and by more or less altered small patches of granitic magmas until approx. 530 to 507 Ma (Table 2). Sediments in the back-arc are mainly paragneisses and micaschists (greywackes) together with some quartzites and breccias (i.e., chert facies; Gilg et al. 1989), whereas dark phyllites and minor amounts of micaschists, quartzites and serpentinites prevail in the fore-arc environment (i.e., shale facies; Gilg et al. 1989).

The basalts can be classified geochemically as volcanic arc basalts due to their trace-element patterns and may be further characterized as active continental margin basalts on the basis of $Zr/Y > 3$ (Höll and Eichhorn 2000). Their geochemical classification is further supported by radiogenic isotope data. Nd and Pb ratios ($\epsilon^t_{CHUR} = 1.3$–9.8; Eichhorn 1995; Eichhorn et al. 1997; $^{206}Pb/^{204}Pb = 18.32$–$18.35$; $^{207}Pb/^{204}Pb = 15.58$; $^{208}Pb/^{204}Pb = 38.07$–$38.12$; Quadt 1985, quoted in Eichhorn et al. 1997) yield values indicative of a volcanic arc geotectonic setting (i.e., values intermediate between mantle- and crustal-dominated ratios). The corresponding Sr ratios reveal a similar signature ($^{87}Sr/^{86}Sr^t = 0.704$; Eichhorn 1995), if not sampled in the vicinity of the Felbertal tungsten deposit where atypically elevated values prevail (due to Sr alteration processes accompanying its formation; Eichhorn et al. 1997). The same pattern is observed in the isotopic ratios of the pyroxenites (Sr-unaltered value: $^{87}Sr/^{86}Sr^t = 0.705$; Eichhorn 1995; $\epsilon^t_{CHUR} = -3.3$–9.0; Eichhorn 1995; Eichhorn et al. 1997; $^{206}Pb/^{204}Pb = 18.39$–$18.58$; $^{207}Pb/^{204}Pb = 15.59$–$15.61$; $^{208}Pb/^{204}Pb = 38.13$–$38.25$; Quadt 1985, compiled in Eichhorn et al. 1997) and granites ($\epsilon^t_{CHUR} = 2.4$–6.7; Eichhorn et al. 1997; $^{206}Pb/^{204}Pb = 18.18$–$18.31$; $^{207}Pb/^{204}Pb = 15.59$–$15.60$; $^{208}Pb/^{204}Pb = 38.14$–$38.15$; Quadt 1985). Unaltered isotopic ratios, REE patterns and calc-alkaline differentiation trends of the gabbros, basalts and granites may be explained by fractional crystallization of a single primary magma of basaltic composition. The formation of a gabbroic to pyroxenitic cumulate on the bottom of a magma chamber would preferentially incorporate Sc and Cr in crystallizing cpx ($\pm$Ni in olivine), which is expressed in markedly elevated

Table 1 Ion-microprobe analytical results for zircons from the Habach terrane. *f206%* 100×(common ^{206}Pb/total ^{206}Pb). *corr* Correction method for common lead: 4 on ^{204}Pb concentration, 8 on ^{208}Pb concentration. *%conc* %concordance = 100×(206/238 age)/(207/206 age)

Grain	Spot description	U (ppm)	Th (ppm)	Th/U	Pb (ppm)	f206%	Pb ratios corrected for common lead						Age (Ma)						Corr.	%Conc.
							206/238	±1S	207/235	±1S	207/206	±1S	206/238		207/235		207/206			
Hornblende-plagioclase gneiss (SG-1)																				
1.1	Bright margin, recryst. sector zoned	120	14	0.12	10	0.55	0.0862	20	0.710	23	0.05977	116	533	12	545	14	595	42	8	89
1.2	Dark center, recryst. sector zoned	285	37	0.13	23	0.46	0.0833	19	0.661	24	0.05751	150	516	11	515	15	511	57	4	101
2.1	Dark center, oscill. zoned	338	52	0.11	29	0.32	0.0884	20	0.709	19	0.05815	67	546	12	544	11	535	25	8	102
2.2	Bright margin, faded oscill. zoned	191	21	0.15	16	0.53	0.0876	20	0.693	20	0.05737	91	541	12	535	12	506	35	8	107
3.1	Bright margin, faded oscill. zoned	205	23	0.11	17	0.55	0.0871	20	0.695	21	0.05786	91	539	12	536	12	525	35	8	103
3.2	Dark center, oscill. zoned	363	87	0.24	32	0.15	0.0911	21	0.751	21	0.05981	78	562	12	569	12	597	28	8	94
4.1	Bright margin, faded oscill. zoned	189	21	0.11	16	0.54	0.0883	20	0.720	21	0.05916	92	545	12	551	12	573	34	8	95
4.2	Dark center, oscill. zoned	164	29	0.18	14	0.79	0.0890	21	0.699	22	0.05696	107	549	12	538	13	490	42	8	112
5.1	Bright outer margin, sector zoned	91	9	0.10	7	1.20	0.0773	19	0.591	23	0.05543	151	480	11	471	15	429	61	8	112
5.2	Dark center, oscill. zoned	564	115	0.20	48	0.00	0.0886	20	0.728	18	0.05958	44	547	12	555	10	588	16	8	93
6.1	Bright margin, faded oscill. zoned	230	30	0.13	21	0.47	0.0939	21	0.755	21	0.05832	81	579	13	571	12	542	30	8	107
6.2	Dark center, oscill. zoned	361	59	0.16	32	0.24	0.0931	21	0.750	20	0.05848	65	574	12	568	11	548	24	8	105
7	Bright margin, faded oscill. zoned	146	18	0.12	13	0.72	0.0893	21	0.722	23	0.05862	112	551	12	552	14	553	42	8	100
8	Bright margin, faded oscill. zoned	92	11	0.12	8	1.41	0.0915	22	0.750	27	0.05946	143	564	13	568	16	584	52	8	97
9	Bright margin, faded oscill. zoned	118	16	0.14	11	1.69	0.0903	21	0.696	25	0.05593	131	557	13	537	15	450	52	8	124
10	Dark center, oscill. zoned	356	52	0.15	30	0.43	0.0879	20	0.716	19	0.05909	66	543	12	548	11	570	24	8	95
11	Dark center, oscill. zoned	151	20	0.14	13	0.94	0.0863	20	0.688	22	0.05783	109	534	12	532	13	523	41	8	102
12	Dark center, oscill. zoned	218	26	0.12	19	0.50	0.0914	21	0.738	21	0.05854	80	564	12	561	12	550	30	8	103
Muscovite gneiss (SG-5)																				
1.1	Partly recrystallized	1,110	130	0.11	77	0.84	0.0718	15	0.539	18	0.05440	127	447	9	438	12	388	52	4	115
1.2	Weak parallel zoning, crack?	659	146	0.22	45	0.73	0.0689	15	0.545	20	0.05734	163	430	9	442	14	505	63	4	85
2	Recrystallized	1,241	45	0.03	70	0.59	0.0603	13	0.453	11	0.05448	48	378	8	380	8	391	20	8	97
3	Mottled mosaic	668	90	0.13	44	0.69	0.0670	14	0.522	19	0.05647	154	419	9	427	13	471	60	4	89
4	Recrystallized	1,568	21	0.01	84	0.64	0.0573	12	0.425	10	0.05387	44	359	8	360	7	366	19	8	98
5	Weakly zoned	2,083	614	0.29	152	0.10	0.0737	15	0.580	13	0.05700	44	459	10	464	9	492	17	4	93
6	Weakly zoned	1,580	460	0.29	118	0.28	0.0748	16	0.585	14	0.05672	64	465	10	468	10	481	25	4	97
7	Weakly zoned	2,083	614	0.29	149	0.00	0.0724	15	0.580	13	0.05809	30	451	9	465	8	533	11	8	85
8	Recrystallized	2,969	1,215	0.40	111	1.03	0.0361	7	0.263	8	0.05291	121	229	5	238	7	325	52	4	70
9	Weakly zoned	2,064	654	0.31	161	0.26	0.0774	16	0.617	14	0.05779	47	481	10	488	9	522	18	8	92
10	Weakly zoned	3,127	1,327	0.42	188	0.08	0.0586	12	0.453	10	0.05602	47	367	8	379	8	453	19	8	81
11	Weakly zoned	1,930	707	0.36	139	0.22	0.0714	15	0.563	13	0.05724	56	445	9	454	9	501	22	4	89
Porphyroid gneiss (SG-8)																				
1	Inherited core, recrystallized	370	86	0.23	96	0.32	0.2512	38	5.547	93	0.16015	86	1,445	20	1,908	15	2,457	9	4	59

2	Xenocryst, faded oscill. zoned	709	43	0.06	35	0.75	0.0520	11	0.381	10	0.05317	69	327	7	328	8	336	30	8	97
3	Xenocryst, strongly zoned	737	225	0.30	66	0.33	0.0874	19	0.721	20	0.05980	82	540	11	551	12	597	30	4	91
4	Strongly zoned	552	51	0.09	24	0.25	0.0467	10	0.335	10	0.05205	83	294	6	293	7	288	37	8	102
5	Recrystallized	513	38	0.07	22	0.17	0.0431	10	0.301	21	0.05064	320	272	6	267	16	225	146	4	121
6	Strongly zoned	313	214	0.68	17	1.86	0.0463	11	0.343	16	0.05373	209	292	7	299	12	360	88	8	81
7	Xenocryst, partly recrystallized	597	325	0.54	34	0.85	0.0529	12	0.382	18	0.05234	203	332	7	329	13	301	89	4	111
8	Xenocryst, strongly zoned	448	77	0.17	29	0.84	0.0652	15	0.500	24	0.05557	223	407	9	411	16	436	90	4	93
9	Strongly zoned	1,341	269	0.20	60	0.34	0.0458	10	0.331	9	0.05238	60	289	6	290	7	302	26	8	96
10	Inherited core, recrystallized	477	240	0.50	75	0.18	0.1412	31	1.926	50	0.09894	112	851	18	1,090	17	1,604	21	4	53
11	Strongly zoned	347	197	0.56	17	2.36	0.0432	10	0.301	29	0.05055	456	273	6	267	23	221	196	4	124
12	Inherited core, partly recrystallized	1,026	197	0.19	85	0.29	0.0854	18	0.672	18	0.05711	71	528	11	522	11	496	27	4	106
13	Inherited core, recrystallized	371	67	0.17	62	0.21	0.1638	36	2.381	61	0.10542	113	978	20	1,237	18	1,722	20	4	57
14	Inherited core, partly recrystallized	496	39	0.07	166	0.18	0.3294	71	7.077	160	0.15582	66	1,835	35	2,121	20	2,411	7	4	76
15	Strongly zoned	521	139	0.26	23	1.07	0.0428	9	0.307	10	0.05211	117	270	6	272	8	290	52	8	93
16	Inherited core, faded oscill. zoned	841	608	0.72	129	0.18	0.1374	29	1.268	30	0.06698	58	830	17	832	14	837	18	4	99
17	Inherited core – rim mixture!	366	90	0.24	28	1.00	0.0756	16	0.579	28	0.05559	226	470	10	464	18	436	91	4	108
Gneiss clast of meta-breccia (SG-4)																				
1.1	Inherited c., unmixed, quenched CL	210	113	0.53	51	0.95	0.2115	33	3.161	72	0.10836	162	1,237	18	1,448	18	1,772	27	4	70
1.2	Faded oscill. zoned, bright CL	82	45	0.54	8	5.88	0.0801	15	0.621	39	0.05622	323	497	9	491	24	461	128	8	108
1.3	Faded oscill. zoned	201	86	0.42	19	4.88	0.0804	13	0.640	24	0.05773	190	499	8	502	15	520	73	8	96
2.1	Inherited core, recrystallized	134	57	0.42	53	0.35	0.3630	59	6.405	127	0.12797	119	1,996	28	2,033	17	2,070	16	8	96
2.2	Strongly zoned	143	48	0.33	12	1.54	0.0805	14	0.636	26	0.05734	199	500	9	500	16	505	77	8	99
3.1	Inherited core, quenched CL	901	8	0.01	73	0.49	0.0877	13	0.714	12	0.05911	45	542	8	548	7	571	17	4	104
3.2	Faded oscill. zoned	219	125	0.57	20	1.96	0.0797	13	0.627	24	0.05706	186	495	8	495	15	494	72	8	100
3.3	Oscill. zoned	307	31	0.09	25	2.32	0.0800	12	0.629	16	0.05706	111	497	8	496	10	494	43	8	100
4.1	Inherited core, strongly zoned	221	360	1.63	112	0.24	0.3718	58	6.361	108	0.12406	65	2,038	27	2,027	15	2,015	9	8	101
4.2	Strongly zoned	196	53	0.27	17	1.89	0.0799	13	0.686	48	0.06229	412	496	8	531	29	684	142	4	72
5.1	Inherited core, recrystallized	269	209	0.77	27	1.20	0.0845	13	0.694	34	0.05952	264	523	8	535	20	586	97	4	89
5.2	Faded oscill. zoned	171	91	0.53	14	1.85	0.0742	13	0.567	44	0.05540	412	462	8	456	29	429	167	4	108
6	Oscillatory zoned	31	73	2.33	5	8.25	0.0812	27	0.696	237	0.06212	2,083	504	17	537	143	678	590	4	74
7	Oscillatory zoned	185	135	0.72	17	1.37	0.0809	13	0.676	38	0.06061	316	502	8	525	23	625	113	4	80
8	Oscillatory zoned	129	139	1.07	14	5.26	0.0788	15	0.507	79	0.04667	713	489	9	417	54	42	322	4	1,176
9.1	Faded parallel zoned, brigth CL	103	87	0.84	10	2.88	0.0808	16	0.645	76	0.05785	663	501	10	506	47	524	254	4	96
9.2	Unmixed zone, quenched CL	2,474	113	0.04	169	0.40	0.0733	10	0.555	8	0.05491	29	456	6	448	6	409	12	8	112

Table 1 (Contd.)

Grain	Spot description	U (ppm)	Th (ppm)	Th/U	Pb (ppm)	f206%	Pb ratios corrected for common lead						Age (Ma)						Corr.	%Conc.
							206/238	±1S	207/235	±1S	207/206	±1S	206/238		207/235		207/206			
10.1	Oscill. zoned, quenched CL	211	30	0.14	16	1.60	0.0785	13	0.578	36	0.05342	312	487	8	464	23	347	132	4	140
10.2	Oscillatory zoned	441	122	0.27	36	0.93	0.0813	12	0.614	22	0.05474	170	504	8	486	14	402	70	4	125
Migmatitic leucosome (SG-3)																				
1	Oscillatory zoned	400	30	0.07	27	0.07	0.0723	8	0.567	17	0.05694	149	450	5	456	11	490	58	4	92
2	Oscillatory zoned	538	34	0.06	38	0.05	0.0756	8	0.586	11	0.05619	81	470	5	468	7	460	32	4	102
3.1	Inherited core, mottled mosaic	318	60	0.18	58	0.15	0.1743	19	3.151	45	0.13111	105	1,036	10	1,445	11	2,113	14	4	49
3.2	Oscillatory zoned	552	36	0.06	40	0.09	0.0772	8	0.611	14	0.05736	108	480	5	484	9	506	41	4	95
3.3	Oscillatory zoned	612	27	0.04	43	0.39	0.0761	8	0.574	15	0.05472	128	473	5	461	10	401	53	4	118
4.1	Inherited core, planar zoned	384	227	0.59	125	0.02	0.2849	30	4.766	57	0.12131	58	1,616	15	1,779	10	1,976	9	4	82
4.2	Weakly recrystallized	329	35	0.10	22	0.58	0.0719	8	0.536	19	0.05414	169	447	5	436	12	377	70	4	119
5	Inherited core, broad planar zoned	60	42	0.69	24	0.16	0.3540	51	6.187	136	0.12675	187	1,954	24	2,003	19	2,053	26	8	95
6.1	Inherited core, quenched CL	1,297	1,899	1.46	150	0.23	0.0868	9	0.708	10	0.05921	55	536	5	544	6	575	20	4	93
6.2	Faded oscill. zoned	553	35	0.06	37	0.38	0.0719	8	0.560	14	0.05648	118	448	5	451	9	471	46	4	95
7.1	Inherited core, partly quenched CL	915	301	0.32	313	1.48	0.3008	30	6.744	72	0.16262	48	1,695	15	2,078	9	2,483	5	8	68
7.2	Oscill. zoned, partly recrystallized	647	127	0.19	47	0.08	0.0745	8	0.581	11	0.05651	83	463	5	465	7	473	33	4	98
8.1	Inherited core, recrystallized	522	242	0.46	47	0.08	0.0835	9	0.710	16	0.06168	116	517	5	545	10	663	40	4	78
8.2	Faded oscill. zoned, bright CL	464	24	0.05	31	0.42	0.0706	8	0.534	14	0.05483	124	440	5	434	9	405	51	4	109
9.1	Inherited core, homogeneous	662	22	0.03	245	0.05	0.3636	37	8.539	92	0.17030	47	1,999	17	2,290	10	2,561	5	4	78
9.2	Oscillatory zoned	1,461	52	0.03	98	0.10	0.0731	7	0.567	7	0.05623	46	455	4	456	5	461	18	4	99
Coarse-grained amphibolite (HG-6)																				
1.1	Recrystallized, mottled mosaic	538	76	0.14	43	4.63	0.0716	8	0.559	13	0.05662	114	446	5	451	9	477	45	8	93
1.2	Dark center, faded oscill. zoned	481	65	0.13	40	3.92	0.0767	9	0.623	14	0.05890	111	476	6	492	9	563	41	8	85
2.1	Faded oscill. zoned	488	62	0.12	37	0.72	0.0780	9	0.615	12	0.05714	80	485	6	487	8	497	31	8	98
2.2	Oscillatory zoned	1,017	108	0.10	77	0.72	0.0783	9	0.607	9	0.05629	54	486	5	482	6	464	21	8	105
3	Recrystallized	235	64	0.27	20	5.93	0.0723	9	0.577	22	0.05791	199	450	6	463	14	526	75	8	86
4.1	Dark center, recrystallized	1,027	19	0.01	79	1.91	0.0783	9	0.608	10	0.05639	58	486	5	483	6	468	23	8	104
4.2	Dark center, recrystallized	1,022	44	0.04	76	0.76	0.0782	9	0.604	9	0.05600	51	486	5	480	6	452	20	8	107
5	Dark center, recrystallized	861	23	0.02	71	0.46	0.0887	10	0.718	10	0.05870	50	548	6	550	6	556	19	8	99
6.1	Oscillatory zoned	744	92	0.12	56	0.53	0.0783	9	0.628	10	0.05816	62	486	6	495	7	536	23	8	91
6.2	Oscillatory zoned	586	47	0.08	44	0.84	0.0777	9	0.616	11	0.05756	72	482	6	488	7	513	28	8	94
7	Dark center, recrystallized	372	124	0.33	33	3.88	0.0773	11	0.580	51	0.05437	465	480	7	465	33	387	193	4	124
8	Dark center, faded oscill. zoned	646	323	0.49	58	4.00	0.0760	9	0.598	16	0.05709	130	473	6	477	10	495	50	8	95

Table 2 Compilation of U-Pb zircon data from various units of the Habach terrane

No.	Name, unit	Geochemistry	Recent geochemical references	Provenance age (Ga)	Formation age (Ma)	U/Pb reference with method applied
Stubach Group (ensialic back-arc basin)						
SG-1	Hornblende-plagioclase gneiss, Basisamphibolit	VAG diorite	Loth and Höll (1994); Loth et al. (1997)		551 ± 9	This work, SHRIMP
SG-2	Coarse-grained amphibolite, Basisamphibolit	VAB gabbro	Quadt (1985, 1992)		539 ± 10	Quadt (1992), conventional dilution
SG-3	Migmatitic leucosome, Serie der Alten Gneise	VAG trondhjemite	Schermaier (1991)	2.64–2.06	530–507	This work, SHRIMP
SG-4	Gneiss clast of meta-breccia, Basisschieferfolge	VAG trondhjemite	Gilg et al. (1989)	2.64–2.06	530–507	This work, SHRIMP
SG-5	Muscovite gneiss, Sturmmannseck	Mantle-diff. granite	Loth and Höll (1994)		530–507	This work, SHRIMP
SG-6	Eclogitic amphibolite, Serie der Alten Gneise	OIB gabbro	Quadt et al. (1997)		488 ± 12	Quadt et al. (1997), convent. and ICP-MS
SG-7	Garnet amphibolite, Zwölferzug	N-MORB gabbro	Quadt (1985)		486 ± 5	Quadt (1985, 1992), conventional dilution
SG-8	Porphyroid gneiss, Sturmmannseck	Post-COL dacitic tuff	Loth and Höll (1994)	2.64–2.06	(279 ± 4), Variscan!	This work, SHRIMP
Habach Group (main volcanic arc)						
HG-1	Fine-grained amphibolite, Eruptivgesteinsfolge	VAB basalt	Schenk and Höll (1989); Thalhammer et al. (1989)		547 ± 27	Eichhorn et al. (1999), SHRIMP
HG-2	Older K2 gneiss, Eruptivgesteinsfolge	VAG granite	Schenk and Höll (1989); Schenk (1990)		547–529	Eichhorn et al. (1999), SHRIMP
HG-3	EOZ gneiss, Eruptivgesteinsfolge	Altered VAG granite	Höll and Eichhorn (2000)		529 ± 17	Eichhorn et al. (1999), SHRIMP
HG-4	Younger K2 gneiss, Eruptivgesteinsfolge	Altered VAG granite	Höll and Eichhorn (2000)		519 ± 14	Eichhorn et al. (1999), SHRIMP
HG-5	Hornblendite, Eruptivgesteinsfolge	Layered high-Mg sill	Eichhorn (1995)		496 ± 2	Quadt (1985, 1992), conventional dilution
HG-6	Coarse-grained amphibolite, Eruptivgesteinsfolge	Gabbroic cumulate	Höck et al. (1993)		482 ± 5	This work, SHRIMP

values of these elements in the trace-element patterns. Continued crystallization of pyroxene would finally lead to an enrichment of the LREE in the differentiated, pyroxene-free melts on top of the magma chamber. Thus, the small patches of granites have to be interpreted as mantle-dominated integral constituents of the rock suite, representing felsic magmatic rocks differentiated from a primary basaltic magma (Thalhammer et al. 1989; Eichhorn et al. 1999; Höll and Eichhorn 2000).

The crystallization age of the gneiss clast of the meta-breccia between 530 and 507 Ma implies a younger sedimentation time, because the trondhjemitic intrusion from which the gneiss clast derived has to be uplifted and eroded. This might be taken as an indication that the prevailing extensional tectonic regime has been reverted into a compressional regime. The sedimentation scenario is probably best described by a successor basin, a deeply subsiding trough filled with predominantly clastic greywacke-arkosic sediments developed after an arc-continent collision and initiated by the uplift of a mountain belt. That successor basin then overlayed the partly eroded, deformed and intruded crystalline complex of the back-arc area (Fig. 5). The mechanism of deposition of the breccias and conglomerates is still a matter of debate. Gilg et al. (1989) considered a deposition by debris and mud flows triggered by local submarine earthquakes and/or a deposition by drifting icebergs. The former interpretation is corroborated by the broad variety of clasts (elongated amphibolites, angular gneisses, calcitic marbles, quartzites, micaschists, hornblende gneisses), the latter by the finds of some exotic, large single clasts which were interpreted as dropstones from melting icebergs, embedded in fine-grained laminated sediments. Such dropstones may be attributed to the prevailing Ordovician Ice Age. The presence of a large ice sheet centered over North Africa (the Ordovician south pole) suggests that the northern margin of Gondwana (including Armorican and Intra-Alpine terranes) remained at high palaeo-latitudes throughout the Ordovician (Tait et al. 1997). The change in deformational style

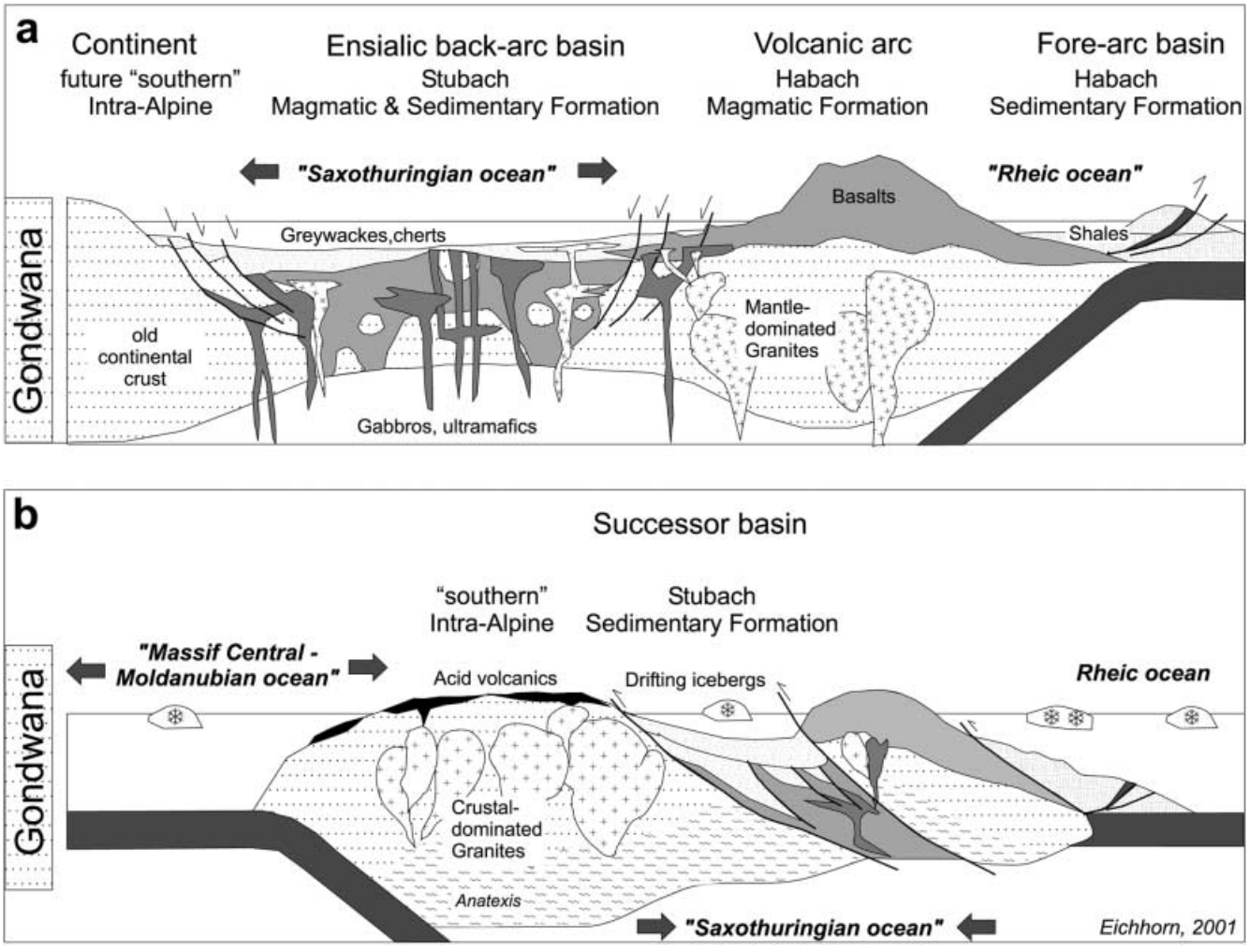

Fig. 5a–b Schematic cross sections through the northern Gondwana margin. **a** The Cambrian. The Habach terrane comprises the various magmatic and sedimentary facies of an Andino-type active margin with ensialic back-arc basin. **b** The Early Ordovician. The extensional tectonic regime has been reverted into a compressional regime, culminating in an arc-continent collision. That orogenic event not only nappe-stacked back-arc, arc and fore-arc rocks closing the narrow oceanic back-arc basin and squeezing ultramafic melts as sills out of high-level magma chambers, but also induced uplift and erosion of deeply rooted crystalline complexes

from extension to compression not only induced uplift and erosion of deeply rooted crystalline complexes. Eichhorn et al. (1999) speculated that mafic to ultramafic cumulates squeezed out of high-level magma chambers between 496 and 486 Ma (Table 2) and intruded as gabbroic to pyroxenitic sills into the arc and back-arc magmatites, while the back-arc region closed during arc-continent collision.

Summary and conclusions

The investigated zircons from the Habach terrane (Central Alps, Austria) indicate a complex chronology of pre-Devonian geological events at 2.64–2.06 Ga, and at ≈830, 551–507, 496–482 and 422–414 Ma: The Archean to Late-Precambrian ages from inherited zircon cores of a migmatitic leucosome, a meta-granitoid clast and a porphyroid gneiss suggest an origin from Gondwana. Rejuvenated magmatic zircons record metamorphic events during Caledonian, Variscan and Alpine orogeneses. The results suggest that the Caledonian metamorphism left the dominant imprint on zircons of the Habach terrane, because Alpine and Variscan upper greenschist- to amphibolite-facies conditions could not even affect the U-Pb isotopic systems in U-rich, and thus highly metamict grains. The Variscan and Alpine metamorphic conditions caused partial lead loss only in zircons of a muscovite gneiss ('white schist'), where extensive fluid flow and brittle deformation enhanced the grains' susceptibility to isotopic disturbance.

From the data it can be concluded that the Habach terrane is the 'missing link' between basement areas of the External domain to the west, and of the Austroalpine domain to the east. In the latter, equivalent units of the Stubach and Habach groups termed 'Speik' and 'Celtic' terranes have been combined under the term 'Noric composite terrane' (Frisch and Neu-

bauer 1989). The Speik terrane is made up of Late-Precambrian to Cambrian magmatic rocks deposited along an active continental margin or in an ensialic island-arc setting. It underwent metamorphism together with the rocks of the Celtic terrane during an Ordovician tectonothermal cycle, thus placing the amalgamation of the Celtic and Speik terranes into Ordovician times. Furthermore, Raumer (1998) already observed remarkable lithostratigraphic parallels between the 'Noric composite terrane' and the northern parts of the Armorican terrane, as both preserve relics of a Cambrian to Ordovician arc/back-arc system. Taking these features into account, it is tempting to compare oceanic crustal relics in the Armorican terrane with relics preserved in the Habach terrane. Relict Amorican 'Rheic' ocean may be found in the Habach sedimentary formation where slices of oceanic crust were scraped off from the subducting oceanic plate to form an accretionary wedge in front of the volcanic arc, and relics of the 'Saxothuringian' ocean, which occur nowadays within a separate sheet situated between the Saxothuringian passive margin sequences and the Tepla-Barrandian zone, may have their equivalents in the ensialic back-arc basin of the Stubach magmatic formation (Fig. 5).

This study demonstrates that the careful selection and handling of single zircon grains can achieve geological meaningful and precise ages in polymetamorphic areas by the combination of careful cathodoluminescence imaging and spot U-Pb age determinations. The Variscan magmatic evolution of the Tauern Window area is already postulated to be similar to the evolution reported from the more westerly Aar, Aiguilles Rouges and Mont Blanc massifs of the External domain (Eichhorn et al. 2000). The present data suggest that this interpretation may be extrapolated to pre-Variscan times and that the list of known terranes with Gondwana affinity can be supplemented by the Habach terrane.

Acknowledgements We would like to thank F. Finger, A. Schermaier, and M. Kupferschmied for providing some of the zircon samples. Zircon preparation and morphological investigation was done at the Institut für Allgemeine und Angewandte Geologie (Ludwig-Maximilians-Universität München), CL imaging in Munich and at the Electron Microscopy Centre (University of Western Australia) in Perth. Zircon analyses were carried out on the sensitive high-resolution ion microprobe spectrometer (SHRIMP II) in Perth during measurement campaigns of R.E. and G.L. in spring 1997 and August 1998. SHRIMP II is operated by a consortium consisting of the Curtin University of Technology, the University of Western Australia, and the Geological Survey of Western Australia, with the support of the Australian Research Council.We are indebted to U. Schaltegger (ETH Zürich), W. Franke (Justus-Liebig-Universität Giessen) and two unknown reviewers for their critical and constructive comments. We wish to express our special gratitude to R. Höll and A. Lagally (Ludwig-Maximilians-Universität München) who substantially improved the manuscript. We gratefully acknowledge the financial support of the Albert-Maucher-Foundation in 1997 and of the Deutsche Forschungsgemeinschaft (DFG) in 1998 (Ho 488/23-1).

References

Claoue-Long JC, Compston W, Roberts J, Fanning CM (1995) Two Carboniferous ages: a comparison of SHRIMP zircon dating with conventional zircon ages and $^{40}Ar/^{39}Ar$ analyses. SEPM Spec Publ 54:3–21

Compston W, Williams IS, Meyer C (1984) U-Pb geochronology of zircons from lunar breccia 73217 using a sensitive high-resolution ion-microprobe. J Geophys Res 89:525–534

Eichhorn R (1995) Isotopengeochemische und geochronologische Untersuchungen an Gesteinen und Mineralen der Scheelit-Lagerstätte Felbertal (Land Salzburg, Österreich). Münchner Geol Hefte 15:1–78

Eichhorn R, Schärer U, Höll R (1995) Age and evolution of scheelite-hosting rocks in the Felbertal deposit (Eastern Alps): U-Pb geochronology of zircon and titanite. Contrib Mineral Petrol 119:377–386

Eichhorn R, Höll R, Jagoutz E, Schärer U (1997) Dating scheelite stages: a strontium, neodymium, lead approach from the Felbertal tungsten deposit, Central Alps, Austria. Geochim Cosmochim Acta 61/23:5005–5022

Eichhorn R, Höll R, Loth G, Kennedy A (1999) Implications of U-Pb SRHIMP zircon data on the age and evolution of the Felbertal tungsten deposit (Tauern Window, Austria). Int J Earth Sci 88:496–512

Eichhorn R, Loth G, Höll R, Finger F, Schermaier A, Kennedy A (2000) Multistage Variscan magmatism in the central Tauern Window (Austria) unveiled by U/Pb SHRIMP zircon data. Contrib Mineral Petrol 139:418–435

Frisch W, Neubauer F (1989) Pre-Alpine terranes and tectonic zoning in the eastern Alps. Geol Soc Am Spec Pap 230:91–100

Gilg HA, Höll R, Kupferschmied MP, Reitz E, Stärk H, Weber-Diefenbach K (1989) Die Basisschieferfolge in der Habachformation im Felber- und Amertal (Tauernfenster, Salzburg). Mitt Österr Geol Ges 81:65–91

Gradstein FM, Ogg J (1996) A Phanerozoic time scale. Episodes 19/1&2:3–5

Hammer W (1937) Bemerkungen zu Blatt Kitzbühel-Zell am See der geologischen Spezialkarte (1:75000). Verh Geol BA 1937:99–108

Heaman LM, Bowins R, Crocket J (1990) The chemical composition of igneous zircon suites: implications for geochemical tracer studies. Geochim Cosmochim Acta 54:1597–1607

Höck V, Kraiger H, Lettner H (1993) Oceanic vs continental origin of the Paleozoic Habach Formation in the vicinity of the Felbertal scheelite deposit (Hohe Tauern, Austria): a geochemical approach. Abh Geol BA 49:79–95

Hoernes S, Friedrichsen H (1974) Oxygen isotope studies on metamorphic rocks of the Western Hohe Tauern (Austria). Schweiz Mineral Petrogr Mitt 54:769–788

Höll R (1975) Die Scheelitlagerstätte Felbertal und der Vergleich mit anderen Scheelitvorkommen in den Ostalpen. Bayer Akad Wissens Math Nat Kl 157a:1–114

Höll R, Eichhorn R (2000) Tungsten mineralization and metamorphic remobilization in the Felbertal scheelite deposit, Central Alps, Austria. Rev Econ Geol 11:233–264

Kupferschmied MP (1994) Geologische Untersuchungen im Tauernfenster zwischen Hollersbachtal und Krimmler Achental. Münchner Geol Hefte 12:1–160

Loth G, Höll R (1994) Zircon morphology and typology studies of rocks from the polymetamorphic Stubach complex (Altkristallin Formation) in the vicinity of the Felbertal tungsten deposit (Eastern Alps) In: Seltmann R, Kämpf H, Möller P (eds) Metallogeny of collisional orogens. Czech Geol Surv, Prague, pp 357–363

Loth G, Höll R, Kennedy A (1997) Origin of banded amphibolites from the Stubach Group (Tauern Window, Eastern Alps): a zircon morphology and U-Pb-SHRIMP study (Abstr). Ber Dtsch Mineral Ges, Beih 1 z Eur J Mineral 9:231

Ludwig KR (2000) User's manual for Isoplot/Ex version 2.2. – a geochronological toolkit for Microsoft Excel. Berkeley Geochronol Center Spec Publ 1a:1–53

Paquette L, Ménot RP, Peucat JJ (1989) REE, Sm-Nd and U-Pb zircon study of eclogites from the Alpine External massifs (Western Alps): evidence for crustal contamination. Earth Planet Sci Lett 96:181–198

Pidgeon RT (1992) Recrystallization of oscillatory zoned zircon: some geochronological and petrological implications. Contrib Mineral Petrol 110:463–472

Pidgeon RT (1997) Gem zircon: a new role as a standard for the measurement of geological time using ion microprobes. Z Dtsch Gemmol Ges 46/1:21–28

Puhl J, Melcher F, Meisel T (1998) Vergleichende geochemische Untersuchungen an ultramafischen Gesteinen der Ostalpen (abstr). Ber Dtsch Mineral Ges, Beih 1 z Eur J Mineral 10:225

Quadt von A (1985) Geochronologische, geochemische und isotopengeochemische Untersuchungen an Gesteinen der Habachformation, der Scheelitlagerstätte und des angrenzenden Altkristallins im Felbertal (Land Salzburg, Österreich). PhD Thesis, University of Zürich

Quadt von A (1992) U-Pb zircon and Sm-Nd geochronology of mafic and ultramafic rocks from the central part of the Tauern Window (Eastern Alps). Contrib Mineral Petrol 110:57–67

Quadt von A, Günther D, Frischknecht R, Zimmermann R, Franz G (1997) The evolution of pre-Variscan eclogites in the Tauern Window (Eastern Alps): a Sm-Nd-, conventional and laser ICP-MS zircon U-Pb study. Schweiz Mineral Petrogr Mitt 77:265–279

Raith JG, Stein HJ, Höll R (2001) Re-Os ages for molybdenites from the Felbertal tungsten deposit, Tauern Window, Austria (Abstr). EUG 11, Strasbourg, France. Terra Abstr 12:263

Raumer von JF (1998) The Paleozoic evolution in the Alps: from Gondwana to Pangea. Geol Rundsch 87:407–435

Reitz E, Höll R (1988) Jungproterozoische Mikrofossilien aus der Habachformation in den mittleren Hohen Tauern und dem nordostbayerischen Grundgebirge. Jahrb Geol BA 131:329–340

Reitz E, Daneck T, Miller H (1989) Ein Nachweis jungproterozoischen Alters von Schwarzphylliten am Tauern-Nordrand (Salzburg, Österreich) und seine Bedeutung für den Bau der Hohen Tauern. Jahrb Geol BA 132:751–760

Schaltegger U (1993) The evolution of the polymetamorphic basement in the central Alps unravelled by precise U-Pb zircon dating. Contrib Mineral Petrol 113:466–478

Schaltegger U, Fanning CM, Günther D, Maurin JC, Schulmann K, Gebauer D (1999) Growth, annealing and recrystallization of zircon and preservation of monazite in high-grade metamorphism: conventional and in-situ U-Pb isotope, cathodoluminescence and microchemical evidence. Contrib Mineral Petrol 134:186–201

Schenk P (1990) Mikrothermometrische gefügekundliche und geochemische Untersuchungen zur Genese der Scheelitlagerstätte Felbertal/Ostalpen. Münchner Geol Hefte 1:1–241

Schenk P, Höll R (1989) Metamorphe hydrothermale Eruptionsbrekzien in der Scheelitlagerstätte Felbertal/Ostalpen (Österreich). Mitt Österr Geol Ges 81:93–107

Schermaier A (1991) Geologisch-petrographische Untersuchungen zur präalpidischen Entwicklung am Ostrand des Venedigermassivs (Hohe Tauern). Jahrb Geol BA 134:345–367

Söllner F, Nelson DR, Miller H (1997) Provenance, deposition and age of gneiss units from the KTB drill hole (Germany): evidence from SHRIMP and conventional U-Pb zircon age determinations. Geol Rundsch 86 (Suppl):235–250

Steiger RH, Jäger E (1977) Subcommission on geochronology: convention on the use of decay constants in geo- and cosmochronology. Earth Planet Sci Lett 36:359–362

Tait JA, Bachtadse V, Franke W, Soffel HC (1997) Geodynamic evolution of the European Variscan fold belt: palaeomagnetic and geological constraints. Geol Rundsch 86:585–598

Thalhammer OAR, Stumpfl EF, Jahoda R (1989) The Mittersill Scheelite Deposit (Austria). Econ Geol 84:1153–1171

Vavra G, Gebauer D, Schmid R, Compston W (1996) Multiple zircon growth and recrystallization during polyphase Late Carboniferous to Triassic metamorphism in granulites of the Ivrea zone (Southern Alps): an ion microprobe (SHRIMP) study. Contrib Mineral Petrol 122:337–358

Williams IS, Buick IS, Cartwright I (1996) An extended episode of early Mesoproterozoic metamorphic fluid flow in the Reynolds range, central Australia. J Metamorph Geol 14:29–47